Effects of Structure and Defect on Fatigue Limit in High Strength Ductile Irons

Jinhak Kim*
Department of Mechanical Engineering, Kangwon National University
Mingun Kim
Division of Mechanical and mechatronices Engineering Kangwon National University

In this paper, the influence of several factors such as hardness, internal defect and non-propagating crack on fatigue limits was investigated with three kinds of ductile iron specimens. From the experimental results the fatigue limits were examined in relation with hardness and tensile strength in case of high strength specimens under austempering treatment; in consequence the marked improvement of fatigue limits were not showed. The maximum defect size was an important factor to predict and to evaluate the fatigue limits of ductile irons. And, the quantitative relationship between the fatigue limits (σ_w) and the maximum defect sizes ($\sqrt{area}_{max}$) was expressed as $\sigma_w{}^n \cdot \sqrt{area}_{max} = C_2$. Also, it was possible to explain the difference for the fatigue limits in three ductile irons by introduction of the non-propagating crack rates.

Key Words : Fatigue, Fatigue Limit Ratio, Maximum Defect Size, Non-Propagating Crack (NPC), High Strength Ductile Irons

1. Introduction

Ductile irons have several engineering and manufacturing advantages to cast steels. These are excellent damping capacity, better wear resistance, 20-40% lower manufacturing cost, and lower volume shrinkage during solidification (Lampamn, 1996). In particular, austempered ductile irons (ADI) offer excellent workability, a mass 10% lower than steel, and a manufacturing cost 20% lower, while for a given hardness it is stronger, more ductile and has a better wear resistance than conventional grade of ductile irons (James, 1999; Park, 1993).

These superior characteristics mean that the ductile irons are widely used in many applications including automobile parts such as torque rod, spindles, exhaust manifold and braking parts. Practically, the evaluation of the fatigue reliability is recognized as one of the important assignments in the ductile irons. The data about this, however, are not in abundance. Especially, there remain uncertain facts in examination for the effects of structural factors on the fatigue limit. For example, the fatigue limit did not improve with the increase of tensile strength and of toughness in the austempered ductile irons. As one of these causes, in austempered ductile irons, it has been pointed out that fatigue crack initiation is very sensitive to local micro structural and mechanical factors (Fukuyama, 1993). That is, it can be assumed that the strengthening of the matrix structure caused by the austempering treatment, increases the sensitivity to the internal defects such as graphite and casting defects, and then decreases the fatigue limits.

The purpose of this work was to investigate the mechanical and structural factors effects on the fatigue limits of three ductile irons in the laboratory air environment. Moreover, quantitative relationship between fatigue limits and estimated

* Corresponding Author,
E-mail : jinhak@kangwon.ac.kr
TEL : +82-361-252-2517 ; **FAX** : +82-361-242-6013
Department of Mechanical Engineering Kangwon National University, 192-1, Chunchon, Kangwon-do 200-701, Korea. (Manuscript **Received** August 23, 1999; **Revised** February 15, 2000)

Table 1 Chemical composition of experimental material (wt.%)

	C	Si	Mn	P	S	Mg	Fe
GCD45	3.75	3.0	0.15	0.03	0.015	0.04	Bal.

Table 2 Typical mechanical properties of the three ductile irons

	σ_Y	σ_B	δ	Hv
Series A	316	443	23.8	221
Series B	507	869	7.8	480
Series C	799	1065	9.4	512

σ_Y: Yield strength, 0.2% proof stress (MPa)
σ_B: Tensile strength (MPa)
δ: Elongation (%)
Hv: Vicker's hardness

maximum defect size in critical surface layer, rates of non-propagating crack (NPC) existing on specimen surface, respectively, were examined together.

2. Experimental Procedure

2.1 Alloy characterisation

The ductile irons specimens were obtained from the commercial grade products (GCD45). Chemical compositions are given in Table 1. Samples were cut and then heat treated prior to final machining. Series A was given a stress relief heat treatment at 600℃ for 2 hours, followed by cooling in air to the room temperature. Series B was austenitized at 900℃ for 1 hour, quenched into a salt bath and held 600℃ for 1 hour, and then cooled in air to the room temperature. Also, series C was austenitized at 900℃ for 1 hour, quenched into a salt bath and held 400℃ for 1 hour, and then cooled in air to room temperature. During the austenitizing process, the transfer of the specimens from the furnace to the salt bath was very rapid, to ensure that the austenite formed at high temperature would not transform to coarse pearlite.

Microscopic photography of their structures are given in Fig. 1, after etching in 3% Nital. The

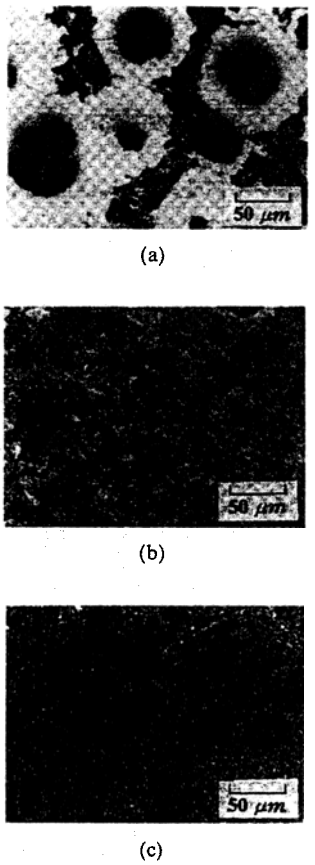

Fig. 1 Typical microstructures, ×200, (a) Series A, (b) Series B and (c) Series C

series A structure is typical bull's eye type (ferrite and pearlite), and the series B structure is predominantly fine pearlite. The series C structure comprises ausferrite (James, 1999) which is the mixture of acicular ferrite and austenite.

Mechanical properties were measured for the three ductile irons and the data are given in Table 2. Results are given as the average values from five tests. Also, hardness are given as the average values from 30 points with the indentation loads of 50 g on the samples.

2.2 Testing conditions

Testing was performed using rotary bending fatigue tester ($R=-1.0$) in laboratory condition. Test frequency was 60 Hz with constant speed of 3600 rpm. Specimens were machined into plain type which have the minimum diameter of 9 mm, and then polished to the mirror surface with the

emery-paper (from #80 to #2000) and the alumina powder (0.3 μm) before tests.

3. Results and Discussion

3.1 Effects of mechanical factors on the fatigue limits

S-N curves for the three ductile irons specimen in laboratory air are shown in Fig. 2. It can be seen that S-N curves are clearly divided horizontal and slope part, resemblant to those of the high strength carbon steels. Also, the distinguished scattering in the fatigue limits (Fukuyama, 1993) did not occur under the same applied stress level. Fatigue limits are estimated to be 191 MPa in series A, 221 MPa in series B and 255 MPa in series C, respectively.

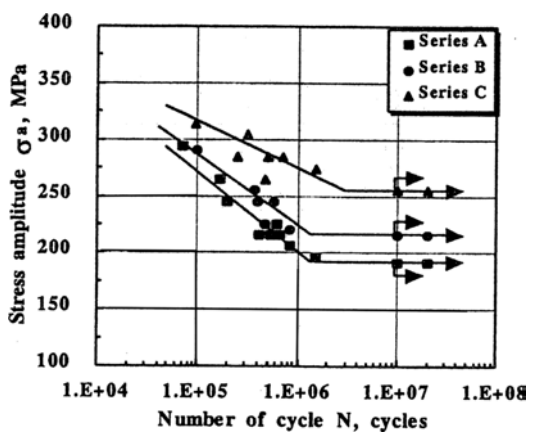

Fig. 2 S-N curves for three specimen series

Then, the relationship between the fatigue limits and the mechanical factors such as hardness and tensile strength are investigated. Fatigue limits for three ductile irons are presented in Fig. 3, plotted against the Vicker's hardness, and also the data of FCD40 (Sugiyama, 1992), ADI100 (Kato, 1997) and FCD60 and FCD70 (Endo, 1988) were put down for reference. Generally, the specimens of steels and irons which have the similar heat treatment history show the similar fatigue behavior. In Fig. 3, the fatigue limits of FCD60 and FCD70 which experienced the same normalizing treatment have an increase tendency in proportion to the Vicker's hardness. Considering that the fatigue limit of series A and that of FCD40 (600℃, 2 hours annealed, σ_B=406 MPa) would have similar fatigue behavior because of the close similar heat treatment history, so it is possible to draw a straight line between those two points. Also, it can be estimated that the fatigue limit of ADI100 has the resemblant tendency. That is, the fatigue limit increases in proportion to the Vicker's hardness. As shown in Fig. 3, the data of ADI100 was in accordance with the straight line.

From Fig. 3, it can be seen that the fatigue limits are improved accompanying by the hardness increase, while in case of the series B and C the expected increment for the fatigue limits are not observed.

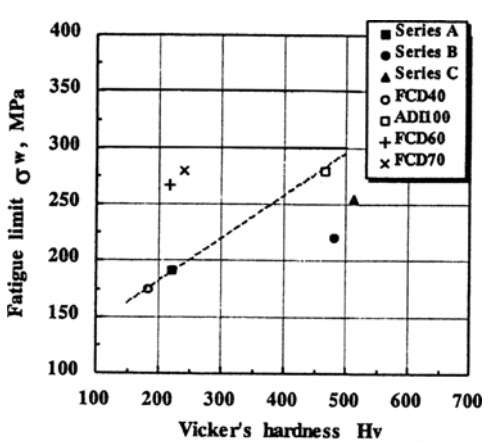

Fig. 3 Relationship between fatigue limits and vicker's hardness

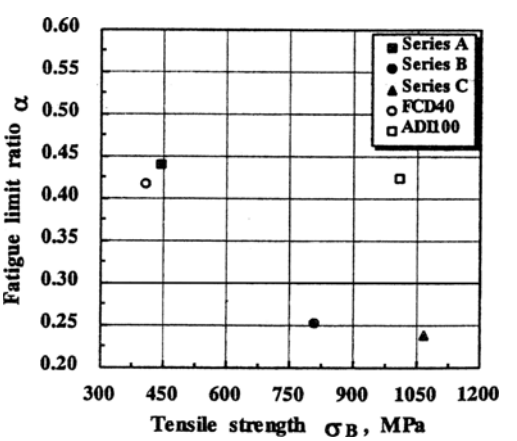

Fig. 4 Relationship between fatigue limits ratio and tensile strength, $\alpha=\sigma_w/\sigma_B$

Figure 4 indicates the variation of the fatigue limit ratio ($\alpha=\sigma_w/\sigma_B$) of the ductile irons. From the figure, it can be seen that the fatigue limit ratio (α) of series A, FCD40 and ADI100 show relatively higher values of 0.40~0.45, while in case of series B and series C show the lower values of 0.20~0.25.

Practically, Fig. 5 shows SEM micrographs of the fatigue crack origins in the fractured specimens for series B and series C. It can be seen that the fatigue crack commenced at a large globular graphite existing just below the surface, and arrow marks mean the fatigue crack origins. It is believed that several fatigue cracks are developed at the ruggedness around the globular graphite nodules, propagate and, eventually, lead to fracture.

It is also believed that the matrix structures of series B and series C are more sensitive to the defects, such as internal graphites and casting defects, than that of series A. This result shows good agreement with the prior report (Kato, 1997) which showed that the defects sensitivity in the high strength ductile irons is higher than in the annealed ductile irons, on the basis of practical experiments performed with artifacts specimens.

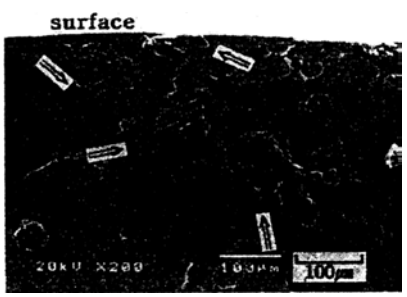

(a)

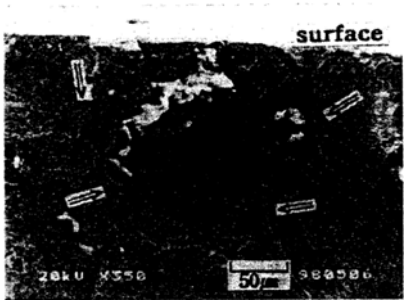

(b)

Fig. 5 SEM micrographs of fracture surface of specimens, (a) Series B(σ_a=248MPa, $N_f=3.2\times10^5$), (b) Series C(σ_a=255MPa, $N_f=1.3\times10^6$)

Also, it can be assumed that, as a results of the increased defects sensitivity and metallurgical variation in local structure caused by heat treatment, in case of series B and series C fatigue limits increases accompanying by the increment of hardness and tensile strength are not acquired.

From the above results, it could be known that the fatigue limits of the ductile irons are improved by the austempering treatment; however, the fatigue limits increment through the austempering treatment should be carried out under the assumption that geometries of the globular graphite nodules, being inherent stress concentration place, should be substantially made better.

3.2 Relationship between fatigue limits and maximum defect sizes

In carbon steels, several non-propagating cracks (NPC, length : 100~500 μm) were observed on the specimens surface which endured the 10^7 cycles under the applied fatigue limit stress. That is, the fatigue limits of the carbon steels are determined in conformity to the critical applied stress amplitude which does not drive the fatigue crack propagation (Murakami, 1993). Therefore, the fatigue limits of the round bar specimens in carbon steels are governed by the longest non-propagating crack, that is a critical non-propagating crack, L_c, among the NPCs existing on the specimens surface. Subsequently, it is well known that the relationship between the fatigue limit (σ_w) and the critical non-propagating crack (L_c) follows the Eq. (2) below (Kim, 1988):

$$\sigma_w^m \cdot L_c = C_1 \tag{2}$$

where a superscript m and C_1 are material constants.

However, in multi-defective materials such as ductile irons and other cast materials, it is very difficult to measure the accurate critical non-propagating crack, L_c. On the other hand, Murakami proposed the following hereditable Eq. (3).

$$\sigma_w = 1.43(H_v + 120)/(\sqrt{area}_{max})^{1/6} \quad (3)$$

where, H_v represents Vicker's hardness, and $\sqrt{area}_{max}$ the estimated maximum defect size by extreme statistics method (ESM).

It is proved that Eq. (3) shows the relationship between the fatigue limit (σ_w) and the maximum defect size ($\sqrt{area}_{max}$), and the prediction errors within 10% in the fatigue limits for the defective materials. Hence, in this study, we have attempted the quantitative evaluation for the fatigue limits in three ductile irons through Eq. (2), directly, by substituting $\sqrt{area}_{max}$ for L_c. Figure 6 shows the estimated maximum defect size by the extreme statistics method (ESM) on the fractured specimens surface for three ductile irons. As results of the above estimation, the estimated maximum defect sizes are 260 μm in case of series A, 302 μm in case of series B and 332 μm in case of series C, respectively. From the Fig. 6, the maximum defect sizes could be estimated by the crossing point of linear regression line and recursive period ($T=617$, $F=99.85\%$), where, T presents S/S_0 in case of $S \gg S_0$, also, S indicates the inspecting cross-sectional area, 55.422 mm^2 and S_0 indicates the measuring area per 1 time, 0.083 mm^2.

Fatigue limits for three ductile irons are presented against the estimated maximum defect size through ESM (Fig. 7). For the references, the data of ADI100, FCD40 and FCD70 (Sugiyama, 1992) were shown together. It can be seen that the relationship between the fatigue limits and the maximum defect size are recurred to a straight line in the log-log scale graph and directly arranged to Eq. (4) which shows good agreement with Eq. (2).

$$\sigma_w^n \cdot \sqrt{area}_{max} = C_2 \quad (4)$$

where the exponent $n=6$ and $C_2=3.06\times10^{16}$. Therefore, it is believed that the fatigue limits (σ_w) and the maximum defect size ($\sqrt{area}_{max}$) for three ductile irons have a quantitative relationship subjected to Eq. (4). From the above results, it can be recognized that the maximum defect sizes in the ductile irons correspond to the critical non-propagating cracks in carbon steels, and also the maximum defect sizes are one of important factors to predict and evaluate the fatigue limits.

On the other hand, Fig. 8 shows the non-propagating cracks (NPC) on the specimen surface which endures 10^7 cycles under the fatigue limit stress. It can be seen that the non-propagating cracks commence at the edge of the graphite nodule and propagate to the adjacent graphite nodule before they stop.

Figure 9 presents the fatigue limits (σ_w) and rates (δ) of the non-propagating cracks which connect adjacent graphite nodules, after the microscopic inspection for the minimum diameter

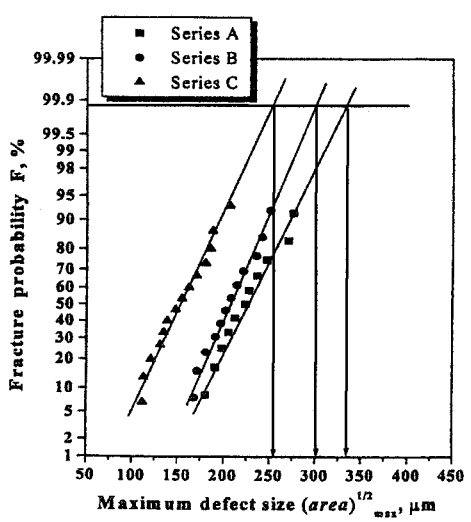

Fig. 6 Estimated maximum defect size for three ductile irons by means of ESM

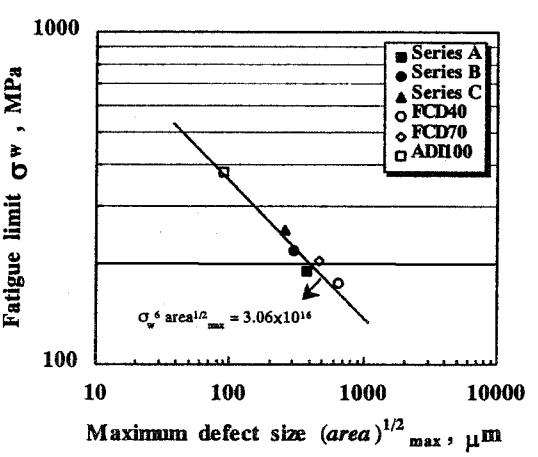

Fig. 7 Quantitative relationship between fatigue limits and maximum defect sizes

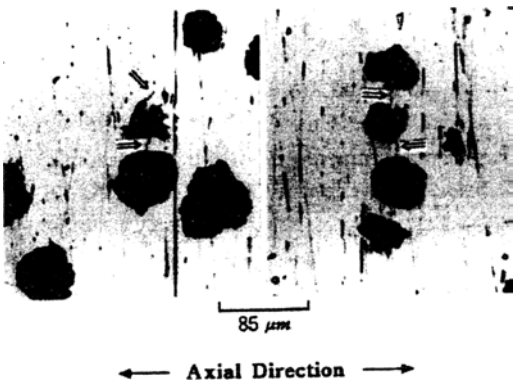

Fig. 8 Non-propagating cracks connecting the adjacent graphite, Series A, σ_a=191 MPa, N= 1.0×10^7

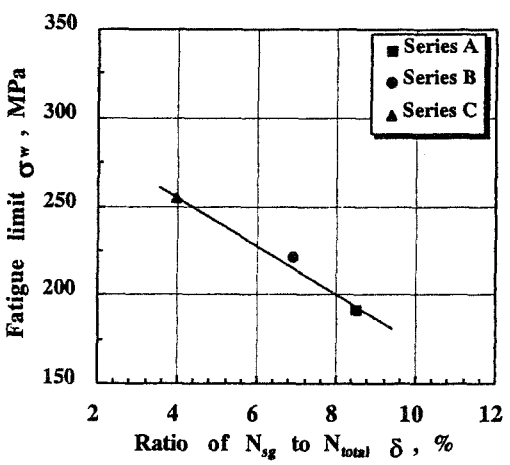

Fig. 9 Difference for the fatigue limits depend on δ ($=N_{sg}/N_{total}$) in specimen series (N_{sg}: Number of NPC connecting the adjacent graphite, N_{total}: Number of total NPC)

range (inspection surface area : 12.78 mm^2) on the unfractured specimens.

It can be seen that the fatigue limits increase in conjunction with the rates decrease. It could be considered that two types of the non-propagating cracks exist. One is that the commenced crack at the globular graphite nodule propagates and then connects the adjacent graphite nodules. The other is that the already initiated crack does not propagate because of the obstacle in the reinforced matrix. It can be assumed that the former has the higher possibility being a short non-propagating crack, and the latter to be a longer non-propagating crack (NPC).

Considering that the critical non-propagating cracks are corresponding to the maximum defect sizes, the difference for the fatigue limits in three ductile irons can be explained by the rates of the non-propagating cracks, which connect the adjacent graphite nodules.

4. Conclusions

From the experimental results, the following conclusions can be made for three ductile irons which have different structures.

(1) As results of investigating the fatigue limits in relation with hardness and tensile strength, the expected high improvement for the fatigue limits, in case of high strength specimens which experienced austempering treatment, are not observed. This reason is that the defect sensitivities of the austempered specimens are higher than that of the annealed.

(2) The estimated maximum defect size is one of the important parameters to predict and evaluate the fatigue limits for the three ductile irons. And, the quantitative relationship between the fatigue limits and the maximum defect sizes can be expressed to $\sigma_w{}^n \cdot \sqrt{area}_{max}=C_2$ (where, n and C_2 are constants).

(3) It is possible to explain the difference of the fatigue limits on the three ductile irons by use of the parameter δ, the rates of the non-propagating cracks.

References

Fukuyama, K., Hasegawa, N., and Nishikawa, Y., 1993, "The Effects of Matrix Structure on Fatigue Life Distribution of Spheroidal Graphite Cast Irons," *Proc. of JSME 70th Conference*, Vol. I, pp. 762～764.

James, M. N. and Wenfong, L., 1999, "Fatigue crack growth in austempered and grey cast irons-stress ratio effects in air and mine water," *Materials Science and Engineering*, A265, pp. 129～139.

Kato, Y. and Takafuji, S., 1997, "Fatigue Strength of Austempered Ductile Cast Iron in a Long Life Regime," *Transactions of the JSME*,

Vol. 63, No. 610, pp. 1153~1158.

Kim, M. G., 1988, "Threshold Condition for the Propagation of Short Fatigue Crack," *Transactions of the KSME*, Vol. 12, No. 3, pp. 505~512.

Lampman, S. R., 1996, Fatigue and Fracture, *ASM Handbook (American Society for Materials)*, Vol. 19, pp. 665~679.

Murakami, Y., 1993, Effects of Small Defects and Nonmetallic Inclusions, *Yokendo LTD.*, pp. 233~258.

Masahiro, E., 1988, "Effects of Graphite Shape Size and Distribution on the Fatigue Strength of Spheroidal Graphite Cast Irons," *Zairyo*, Vol. 38, No. 433, pp. 19~24.

Park, H. S. and Jin, D. K., 1993, "A Study on Corrosive Wear Characteristics and the Mechanism of Austempered Low-Alloy Ductile Iron," *Transactions of the KSME*, Vol. 17, No. 6, pp. 1404~1411.

Sugiyama, Y., Asami, K. and Matsuka, S., 1992, "Quantitative Evaluation Method of Fatigue Limit of Materials with Defects and its Investigation using Ductile Cast Iron," *Transactions of the JSME*, Vol. 58, No. 556, pp. 2287~2292.